THE ASTRONOMICAL JOURNAL, 117:521–533, 1999 January
© 1999. The American Astronomical Society. All Rights Reserved. Printed in U.S.A.

RADII AND EFFECTIVE TEMPERATURES FOR G, K, AND M GIANTS AND SUPERGIANTS

G. T. VAN BELLE AND B. F. LANE
Jet Propulsion Laboratory, California Institute of Technology, 4800 Oak Grove Drive, MS 306-388, Pasadena, CA 91109

R. R. THOMPSON
Department of Physics and Astronomy, University of Wyoming, Laramie, WY 82071

A. F. BODEN, M. M. COLAVITA, P. J. DUMONT, D. W. MOBLEY, D. PALMER, M. SHAO, G. X. VASISHT, AND J. K. WALLACE
Jet Propulsion Laboratory, California Institute of Technology, 4800 Oak Grove Drive, MS 306-388, Pasadena, CA 91109

M. J. CREECH-EAKMAN, C. D. KORESKO, S. R. KULKARNI, AND X. P. PAN
California Institute of Technology, 4800 Oak Grove Drive, MS 306-388, Pasadena, CA 91109

AND

J. GUBLER
Department of Physics, and Center for Astrophysics and Space Sciences, C 0424, University of California, San Diego, La Jolla, CA 92093-0424
Received 1998 June 12; accepted 1998 September 17

ABSTRACT

Interferometrically determined angular diameters obtained at the Palomar Testbed Interferometer (PTI) for 69 giant and supergiant stars are presented. Spectral types of the 59 giant stars generally lie between G6 and M6, although a B7 giant is included; the nine bright giants and supergiants have spectral types between F5 and M5. Comparison of the results to those from the IR Optical Telescope Array interferometer indicate no statistically significant difference between the two data sets. The use of *Hipparcos* parallaxes allows us to measure linear sizes directly for these stars, which range in size from 10 to 260 solar radii. In conjunction with previous results as reported by Dyck et al., the total of 113 giant stars provides empirically determined dependencies of effective temperature and linear radius upon spectral type and $V-K$ color.

Key words: infrared: stars — stars: fundamental parameters — stars: late-type — techniques: interferometric

1. INTRODUCTION

Interferometric observations of giant and supergiant stars have begun to be reported in the literature with an increasing frequency as optical and infrared interferometers come on-line and mature. Observers at installations such as the Mark III Interferometer, IOTA (IR Optical Telescope Array), NPOI (Navy Prototype Optical Interferometer), and PTI (the Palomar Testbed Interferometer) have been utilizing their capability to resolve stars in the <20 mas range to produce a large body of results on evolved stars. These results are significant in that they constitute direct measurements of the parameters of stars that populate the coolest, most luminous portion of the H-R diagram. Efforts over the past year to characterize and utilize PTI have resulted in a large body of data. In this paper we report new visibility observations for 69 evolved stars obtained at PTI. The recent release of the Hipparcos Catalogue (Perryman et al. 1997) has had the added benefit of allowing many of the observed angular sizes to be interpreted as linear radii as well, which dramatically increases the number of stars for which linear sizes have been measured. Together with the previous angular size results obtained at IOTA as reported in Dyck et al. (1996, hereafter Paper I) and Dyck, van Belle, &Thompson (1998, hereafter Paper II), we have been able to characterize empirically the effective temperature and linear radii as a function of spectral type and color.

2. OBSERVATIONS

2.1. *The Interferometer*

PTI is a three-aperture interferometer located at Palomar Observatory in San Diego County, CA. Two of the 40 cm apertures may be used in conjunction for any single interferometric observation. The north and south piers used in this investigation are 110 m apart on a baseline 20° east of true north; the west pier (now operational, but not used for this paper) provides 86 m. Light from the two telescopes being linked interferometrically is reflected by transport optics into a central beam combining laboratory, where two delay lines are located. One of the two delay lines operates as a "move-and-hold" element in the beam train for one of the telescopes, while the second moves dynamically during an observation with a precision of 10–20 nm. Following the delay line elements, the starlight is directed onto a beam combination table, where a dichroic splits off the visible light for tip-tilt sensing using a quad cell incorporating four fiber-fed avalanche photodiodes. After the dichroic, the two telescope beams are combined at a beam splitter. One of the two outputs from the beam splitter is fed directly into a Dewar onto a single pixel of a NICMOS3 detector; this signal is referred to as the "white-light channel." The other output is fed through a single-mode fiber and a prism outside the Dewar, then onto 7 pixels on the detector chip; this signal constitutes the "spectrometer channels." Effective integration time for each pixel is ~ 6.75 ms. The white-light channel is utilized for fringe tracking in a manner similar to that used at the Mark III interferometer as described in Shao et al. (1988).

The channels used for visibility amplitude measurements reported herein are the spectrometer channels, which range in seven 0.07 mm bins across the K band centered at 1.99, 2.06, 2.13, 2.20, 2.27, 2.34, and 2.41 mm. (A new experimental setup for the 1998 observing season onward will have five, not seven, spectral channels.) These channels, having been spatially filtered by a single-mode fiber before detection, were considerably less noisy than the white-light channel. Owing to low flux levels, the 2 edge spectrometer pixels were dropped; the results from the remaining 5 pixels were averaged, resulting in an effective white-light K-band measurement, of wavelength $\lambda = 2.19 \pm 0.01$ mm. For a more complete description of the instrument, see Colavita et al. (1999).

2.2. *Data Reduction*

The PTI calibration code performs data sorting, averaging, and comparison on selected objects. The user identifies a set of science targets to be calibrated and a set of calibration objects to be used as references for the calibration. For the calibration objects, positions and model uniform-disk diameters (the calibration objects are assumed to be single stars) are required as input. The code selects calibration scans that are within user-defined temporal and possibly spatial constraints of a given science target scan and estimates the system visibility, $V^2_{\rm sys}$, for individual calibration scans based on the ratio of the measured and expected V^2 for the calibration object. For potentially resolved calibrators this expected V^2 calculation must include both wavelength and baseline projection effects. Multiple estimates of the system visibility from a single calibrator are weight-averaged to determine a single system visibility estimate, and then estimates from multiple calibration objects are weight-averaged to compute a final ensemble system visibility estimate applied to the science target scan. During the multiple calibrator averaging, system visibility estimates from individual calibrators are intercompared for consistency and flagged or possibly rejected if they disagree beyond a user-defined consistency threshold. Uncertainties in the system visibility and the calibrated target visibility are inferred from internal scatter among the data in a scan and standard error-propagation calculations. The calibration code can be used to calibrate a single night's data or many nights of PTI data spanning an arbitrary length of time. There are versions of the calibration code that perform calibration of both the synthetic wideband and individual spectrometer channel visibilities.

The primary calibrator objects were main-sequence or supergiant stars which are expected to be nearly unresolved by the interferometer (less than 0.75 mas). Given that even these objects would have their disks marginally resolved, the observed calibrator V^2 values were increased slightly for expected angular size. These adjustments were less than 5%, however, since a 0.75 mas object would have a V^2 of roughly 0.95. Expected angular size was based upon a blackbody radiator angular size inferred from available broadband photometry, particularly in the near-infrared (Gezari et al. 1996). Clearly, many stars deviate sharply from blackbody behavior (as will be shown in § 4); however, the hot stars ($T_{\rm eff} > 5000$ K) selected as primary calibrators should not deviate sharply from blackbody behavior. Our experience with reducing the interferometric data has indicated that this technique is more robust than estimating angular size from spectral type–inferred linear radii coupled with distance. The primary calibrators are listed in Table 1. We note that one of our primary calibrators is 51 Peg; despite its noted radial velocity variability, an extensive interferometric campaign to detect V^2 variations has indicated this object is stable at a level of $\Delta V^2 = 0.015$ (Boden et al. 1998).

TABLE 1

PRIMARY CALIBRATION STARS FOR THE SURVEY

Name	HD	Spectral Type	References	$\theta_{\rm BBR}$ (mas)
γ Tri	14055	A1 V	1	0.38 ± 0.08
41 Ari	17573	B8 V	2	0.31 ± 0.07
ν Tau	28024	A8 V	1	0.63 ± 0.07
σ Cyg	202850	B9 Iab	3	0.26 ± 0.07
51 Peg......	217014	G2–3 V	4, 5	0.73 ± 0.05

REFERENCES.—(1) Cowley et al. 1969; (2) Garrison & Gray 1994; (3) Morgan, Whitford, & Code 1953; (4) Houk 1995; (5) Boden et al. 1998.

Secondary calibrator objects were giant stars that were also expected to be nearly unresolved by the interferometer (less than 0.90 mas) but less so than the primary calibrators; a 0.90 mas object has an expected V^2 of 0.90. Angular sizes of these objects were estimated from spectral types and distances *but verified* based upon nearby primary calibrator objects. The purpose of secondary calibrators was to allow science targets to be selected from around the sky even if a primary calibrator was not within 15°; secondary calibrators allow for extension of sky coverage with nearby calibrators, albeit with lower accuracy as the error bars propagate.

Science objects that had more than one calibrator nearby in time (± 1 hr) and space (0°–15°) utilized all calibration visibilities in a weighted sense, based upon locality and statistical weight. For those objects with two or more calibrators, separate normalizations were calculated and compared for consistency. In this fashion both the system performance as characterized by the calibrator visibility, and adjustments to calibrator visibility were established as consistent. Roughly 80% of the science targets observed had two nearby calibration objects; half of those had three or more calibration objects nearby.

Assuming a uniformly irradiating disk, once a normalized value for V^2 has been obtained, an angular size can be obtained by fitting $V^2 = [2J_1(x)/x]^2$, where $x = \theta_{\rm UD} \pi B/\lambda$. The normalized values for V^2 for each observation are listed in Table 2, with their associated observation Julian Date, hour angle, and projected interferometer baseline; in Table 3, the derived uniform disk angular sizes for individual stars are listed. Given the expected departures from a uniform disk (primarily the presence of limb darkening), this assumption is not exactly accurate. We will adjust for that in § 3, noting that expected departures will be small (see Paper II; Tuthill 1994). Since the uniform disk function repeats at low visibility levels, care must be taken to utilize only the monotonic region of the function, found at spatial frequencies for which $V^2 > 0.017$; for the 110 m baseline of PTI, this corresponds to $\theta_{\rm UD} = 4.34$ mas.

2.3. *Target Selection*

Target selection was accomplished by collecting as large a sample of potential targets as possible. First, The Catalog of Infrared Observations (Gezari et al. 1996) was scanned for all measurements with $m_K < 5$ in the proper declination range ($0° < \delta < 55°$). A cross-correlation of the resultant list with the SIMBAD database then allowed for a further cut for those objects with $m_V < 7$, owing to limitations in the star acquisition system at the time of the observations. The general object types as reported by SIMBAD and spectral

TABLE 2

NORMALIZED VISIBILITIES OF STARS OBSERVED AT PTI

Name	JD −2,400,000	HA	B_P (m)	V_N^2
HR 79	50,737.77	−0.08	109.8	0.384 ± 0.017
HR 259	50,737.79	−0.13	108.3	0.107 ± 0.004
HR 274	50,737.79	−0.09	109.3	0.299 ± 0.033
HR 351	50,737.80	−0.04	106.9	0.693 ± 0.022
HR 389	50,737.81	−0.11	109.3	0.485 ± 0.020
HR 450	50,737.82	0.07	105.5	0.446 ± 0.015
HR 564	50,737.83	−0.13	109.1	0.255 ± 0.008
HR 631	50,737.84	−0.25	106.8	0.101 ± 0.003
HR 736	50,737.85	−0.24	109.7	0.357 ± 0.035
HR 882	50,737.88	0.08	109.8	0.528 ± 0.024
HR 1343......	50,737.90	−0.86	109.6	0.744 ± 0.040
HR 1409......	50,737.92	−0.64	107.6	0.382 ± 0.017
HR 1533......	50,737.93	−0.72	109.3	0.263 ± 0.022
HR 1551......	50,737.93	−0.68	109.5	0.302 ± 0.019
HR 1739......	50,737.95	−0.76	108.7	0.753 ± 0.041
HR 1791......	50,737.96	−0.59	109.6	0.694 ± 0.036
HR 1995......	50,737.00	0.01	109.6	0.560 ± 0.046
	50,737.98	−0.42	109.3	0.571 ± 0.036
HR 2012......	50,743.99	0.06	109.6	0.301 ± 0.011
	50,744.95	−0.62	109.1	0.303 ± 0.009
HR 2189......	50,738.01	0.00	109.7	0.255 ± 0.016
HR 2219......	50,738.02	0.14	109.2	0.505 ± 0.032
HR 2630......	50,728.02	−1.34	109.7	0.725 ± 0.065
HR 2696......	50,738.04	−0.33	109.3	0.266 ± 0.030
HR 2805......	50,738.03	−0.71	108.7	0.583 ± 0.060
HR 5215......	50,621.76	2.56	109.4	0.389 ± 0.009
HR 5429......	50,621.77	2.17	108.3	0.085 ± 0.001
HR 5510......	50,621.77	2.07	109.0	0.536 ± 0.009
HR 5638......	50,621.78	1.88	106.8	0.756 ± 0.011
HR 5681......	50,621.79	1.86	109.1	0.328 ± 0.004
HR 5709......	50,621.79	1.88	108.1	0.828 ± 0.013
HR 5745......	50,621.79	1.84	106.3	0.440 ± 0.007
HR 6107......	50,621.84	1.98	109.2	0.100 ± 0.002
HR 6208......	50,623.79	0.61	107.3	0.813 ± 0.017
HR 6258......	50,621.83	1.41	108.3	0.456 ± 0.020
HR 6584......	50,621.90	2.16	108.6	0.475 ± 0.014
HR 6695......	50,621.91	2.08	109.7	0.223 ± 0.007
HR 6820......	50,621.92	2.23	104.5	0.741 ± 0.012
	50,623.86	0.69	105.9	0.706 ± 0.023
HR 7237......	50,621.93	1.58	108.8	0.472 ± 0.008
HR 7238......	50,621.94	1.68	108.5	0.428 ± 0.009
HR 7515......	50,621.94	1.12	109.8	0.817 ± 0.022
	50,690.73	0.65	109.8	0.825 ± 0.019
	50,690.78	1.75	109.7	0.824 ± 0.015
	50,691.72	0.32	109.8	0.788 ± 0.033
	50,691.76	1.38	109.8	0.818 ± 0.018
	50,692.71	0.26	109.8	0.821 ± 0.013
	50,692.76	1.37	109.8	0.824 ± 0.013
HR 7517......	50,621.94	1.12	109.8	0.817 ± 0.022
	50,623.97	1.97	109.7	0.819 ± 0.010
	50,624.00	2.62	109.7	0.815 ± 0.028
	50,690.73	0.65	109.8	0.825 ± 0.019
	50,690.78	1.75	109.7	0.824 ± 0.015
	50,691.72	0.32	109.8	0.788 ± 0.033
	50,691.76	1.38	109.8	0.818 ± 0.018
	50,692.71	0.26	109.8	0.821 ± 0.013
	50,692.76	1.37	109.8	0.824 ± 0.013
	50,693.68	−0.50	109.5	0.801 ± 0.016
HR 7759......	50,726.69	1.41	109.8	0.241 ± 0.021
HR 7834......	50,736.59	−0.44	109.7	0.746 ± 0.024
HR 7847......	50,736.60	−0.38	109.6	0.808 ± 0.039
HR 7942......	50,736.61	−0.28	109.7	0.439 ± 0.017
HR 7995......	50,736.63	0.01	108.8	0.716 ± 0.086
HR 8008......	50,622.94	−0.14	109.2	0.405 ± 0.011
HR 8044......	50,736.64	0.06	106.0	0.187 ± 0.007
HR 8306	50,736.64	−0.56	108.7	0.184 ± 0.011
	50,737.68	0.37	109.5	0.192 ± 0.015
HR 8555	50,690.81	−0.19	109.7	0.721 ± 0.015
	50,691.87	1.24	109.0	0.722 ± 0.025
	50,692.73	−2.05	108.5	0.719 ± 0.017
	50,692.79	−0.67	109.8	0.719 ± 0.014
HR 8684	50,736.66	−1.27	109.7	0.353 ± 0.016
	50,736.69	−0.42	108.8	0.370 ± 0.015
	50,737.69	−0.38	108.7	0.358 ± 0.021
HR 8796	50,623.96	−1.61	109.8	0.464 ± 0.008
HR 8930	50,736.70	−1.01	108.6	0.649 ± 0.029
	50,737.70	−0.97	108.6	0.616 ± 0.037
HR 8942	50,736.66	−1.82	109.8	0.087 ± 0.004
	50,736.71	−0.79	108.4	0.098 ± 0.004
	50,737.71	−0.69	108.2	0.107 ± 0.003
HR 8953	50,736.67	−1.67	109.8	0.376 ± 0.012
	50,737.71	−0.61	109.0	0.384 ± 0.017
HR 9035	50,736.68	−1.85	109.8	0.389 ± 0.018
	50,736.72	−0.78	108.6	0.411 ± 0.011
	50,737.72	−0.69	108.5	0.421 ± 0.018
HR 9055	50,736.74	−0.41	108.2	0.414 ± 0.023
	50,737.76	0.07	107.3	0.437 ± 0.008
IRC +20092......	50,737.92	−0.86	108.9	0.424 ± 0.025
IRC +30086......	50,737.90	−0.84	109.8	0.417 ± 0.015
IRC +30105......	50,737.94	−0.72	109.8	0.276 ± 0.010
IRC +30115......	50,744.93	−0.80	109.8	0.212 ± 0.007
IRC +30309......	50,621.89	2.11	107.3	0.272 ± 0.004
IRC +30412......	50,622.93	0.49	107.8	0.279 ± 0.004
IRC +30438......	50,736.61	−0.22	109.3	0.376 ± 0.014
IRC +30465......	50,622.94	−0.15	109.7	0.487 ± 0.012
IRC +30468......	50,622.94	−0.12	109.0	0.514 ± 0.011
IRC +40018......	50,737.80	−0.01	109.6	0.425 ± 0.031
IRC +40022......	50,737.82	−0.01	109.8	0.391 ± 0.015
IRC +40254......	50,621.76	2.28	109.5	0.702 ± 0.023
IRC+ 40337......	50,621.93	1.49	109.8	0.775 ± 0.017
	50,690.73	1.11	109.8	0.764 ± 0.029
	50,690.77	2.20	109.8	0.761 ± 0.027
	50,691.70	0.59	109.7	0.782 ± 0.026
	50,691.75	1.71	109.8	0.778 ± 0.019
	50,692.70	0.72	109.7	0.780 ± 0.015
	50,692.75	1.88	109.8	0.772 ± 0.012

NOTE.—JD is the Julian date of the observation; HA is the hour angle; B_P is the projected baseline; V_N^2 is the normalized visibility squared.

types were used to obtain yet a further cut of those objects reasonably expected to be luminosity class I, II, or III stellar objects. Angular sizes were then estimated based upon one of two methods: either (1) selection as above for calibrators, where spectral types were used in estimating linear radius, and combined with *Hipparcos* distances to obtain angular size or (2) photometry as reported by SIMBAD was utilized in estimating bolometric flux and then combined with effective temperatures as expected by spectral type to obtain an angular size estimate. Those objects that met the requirement for resolvability by PTI ($1.1 < \theta_{\rm est} < 4.3$ mas, where a 1.1 mas object will have $V^2 \sim 0.85$ for PTI) were then eligible for the observing list. Given the constraints of available observing time for this observing season and the large number of potential science targets, objects that crossed the meridian 10° to either side of the zenith ($21° < \delta < 41°$) were given priority in the observing queue to minimize observing airmass. Given the more than adequate results from the interferometer observing these objects at large

TABLE 3
UNIFORM DISK ANGULAR SIZES

Name	θ_{UD}
HR 79	2.46 ± 0.05
HR 259	3.59 ± 0.10
HR 274	2.74 ± 0.11
HR 351	1.60 ± 0.07
HR 389	2.17 ± 0.06
HR 450	2.37 ± 0.05
HR 564	2.90 ± 0.06
HR 631	3.67 ± 0.11
HR 736	2.54 ± 0.11
HR 882	2.04 ± 0.07
HR 1343	1.41 ± 0.13
HR 1409	2.51 ± 0.06
HR 1533	2.87 ± 0.08
HR 1551	2.73 ± 0.06
HR 1739	1.39 ± 0.13
HR 1791	1.56 ± 0.11
HR 1995	1.93 ± 0.08
HR 2012	2.73 ± 0.06
HR 2189	2.88 ± 0.06
HR 2219	2.11 ± 0.09
HR 2630	1.47 ± 0.21
HR 2696	2.86 ± 0.10
HR 2805	1.90 ± 0.17
HR 5215	2.45 ± 0.05
HR 5429	3.72 ± 0.12
HR 5510	2.03 ± 0.05
HR 5638	1.41 ± 0.06
HR 5681	2.65 ± 0.06
HR 5709	1.15 ± 0.07
HR 5745	2.37 ± 0.05
HR 6107	3.60 ± 0.10
HR 6208	1.21 ± 0.06
HR 6258	2.27 ± 0.06
HR 6584	2.21 ± 0.05
HR 6695	3.00 ± 0.07
HR 6820	1.51 ± 0.06
HR 7237	2.22 ± 0.05
HR 7238	2.35 ± 0.05
HR 7517	1.15 ± 0.06
HR 7759	1.16 ± 0.06
HR 7806	2.93 ± 0.08
HR 7834	1.40 ± 0.08
HR 7847	1.20 ± 0.14
HR 7942	2.30 ± 0.05
HR 7995	1.51 ± 0.28
HR 8008	2.41 ± 0.05
HR 8044	3.26 ± 0.08
HR 8306	3.17 ± 0.07
HR 8555	1.49 ± 0.06
HR 8684	2.54 ± 0.06
HR 8796	2.22 ± 0.05
HR 8930	1.75 ± 0.07
HR 8942	3.62 ± 0.10
HR 8953	2.48 ± 0.05
HR 9035	2.41 ± 0.05
HR 9055	2.36 ± 0.05
IRC +20092	2.36 ± 0.07
IRC +30086	2.36 ± 0.05
IRC +30105	2.81 ± 0.06
IRC +30115	3.04 ± 0.07
IRC +30309	2.89 ± 0.06
IRC +30412	2.85 ± 0.06
IRC +30438	2.49 ± 0.06
IRC +30465	2.16 ± 0.05
IRC +30468	2.09 ± 0.05
IRC +40018	2.34 ± 0.09
IRC +40022	2.44 ± 0.05
IRC +40254	1.54 ± 0.07
IRC +40337	1.31 ± 0.06

hour angles (HA > 2), this appears to have been an arbitrary limitation on the source list and will be discontinued in the future.

2.4. *Night-to-Night Repeatability*

Utilizing nightly weighted average values for normalized V^2, the average standard deviation from night to night was found to be $\Delta V^2 = 0.018$ for stars that were observed on at least three nights. This represents a variety of seeing conditions and calibration sources for the stars. The primary limitation appears to be the degree to which angular sizes of calibration sources can be determined, based upon known spectral types and photometric information for these sources. By way of comparison, the experimental setup utilized at the IOTA interferometer provided a night-to-night measurement accuracy of roughly $\Delta V = 0.051$ (Paper II). The reason for this improvement in normalized visibility is due in part to the use of a single-mode fiber in the PTI beam train; a related experimental setup of the IOTA facility produced comparable results (Perrin et al. 1995). Although these are slightly different observables, each represents a direct measure of the night-to-night repeatability of each instrument's data products in an absolute sense.

2.5. *Comparison to Previous Results*

Unfortunately, there are few results in the literature with which to compare to the results from PTI. We will compare general results (e.g., spectral type vs. effective temperature) in § 3; however, there are only seven specific examples of stars with angular sizes in both the literature and in our data set. Of these, four are inferred diameters from the infrared flux method (IRFM; see Blackwell, Shallis, & Shelby 1979); three are measurements from occultations and interferometry. These data points are listed in Table 4.

The dearth of comparative data points has a twofold explanation. First, interferometrically determined diameters available in the literature are few in number. Second, aggravating the problem presented by the limited data generally available, PTI's stellar disk angular resolution is slightly finer than previously available to interferometry (in the 1–4 mas range, as opposed to the 4+ mas range). Hence, the stars examined with PTI are slightly smaller in physical size, which in turn translates to stars of a slightly earlier spectral type than observed with other interferometers, such as IOTA, IRMA, CERGA, and the Mark III. Some stars of later spectral type (M0 on) were observed with PTI, but this is a function of its greater infrared sensitivity (roughly 2 mag better at K than the experimental setup at IOTA utilized in Papers I and II).

The IRFM sizes and temperatures are in good agreement with the PTI data and error bars, noting that errors were not given for the IRFM numbers. The temperatures are, on average, less than 1 σ away from those measured with PTI; the IRFM angular sizes are between 1 and 2 σ away from the PTI angular sizes. Our diameter for HR 2630 is consistent with the upper limit determined by Richichi et al. (1996) from lunar occultation. The previous interferometric results, however, bear some close examination.

For HR 1791, the value of 1.15 ± 0.05 mas (Mozurkewich et al. 1991) appears to be in contradiction to the PTI value of 1.56 ± 0.11 mas. However, upon closer examination, these authors state that the systematic errors could potentially be considerably larger than the formal errors quoted in the paper. Furthermore, the angular size for this object,

TABLE 4

COMPARISON OF PREVIOUSLY ESTIMATED OR MEASURED TEMPERATURES AND ANGULAR SIZES TO THOSE OBTAINED WITH PTI

Star	Method	$T_{\rm eff}$ (K)	PTI $T_{\rm eff}$ (K)	Size (mas)	PTI Size (mas)	References	Notes
HR 5681......	IRFM	4840	5091 ± 263	2.699	2.65 ± 0.06	1	
HR 8684......	IRFM	4964	5017 ± 425			2	
HR 5429......	IRFM	4298	4470 ± 228	3.825	3.72 ± 0.12	3	
HR 5681......	IRFM	4801	5091 ± 263	2.769	2.65 ± 0.06	3	
HR 8684......	Interferometry			4.9 ± 0.4	2.54 ± 0.06	4	
HR 1791......	Interferometry			1.15 ± 0.05	1.56 ± 0.11	5	Systematic errors might be larger than stated formal error
HR 2630......	Occultation			<1.5	1.47 ± 0.21	6	

REFERENCES.—(1) Blackwell et al. 1979; (2) Castelli et al. 1997; (3) Blackwell & Lynas-Gray 1994; (4) Hutter et al. 1989; (5) Mozurkewich et al. 1991; (6) Richichi et al. 1996.

obtained with the Mark III interferometer, does not appear to have been directly obtained from interferometric data but rather adopted indirectly from surface brightness assumptions. For HR 8684, the value of 4.9 ± 0.4 mas given by Hutter et al. (1989) is strikingly different from our measurement of 2.54 ± 0.06 mas. However, we simply point out that, given the bolometric flux of this object, the larger angular size implies an effective temperature of ~3600 K. This is roughly 1200 K cooler than the temperature expected for a G8 III star (see discussion in § 4.1 and Table 7), which is the well-determined spectral type for the star (Morgan & Keenan 1973). We submit that the previously reported angular size is erroneous. Furthermore, the temperature that is obtained from PTI data (~5000 K) is consistent with both the spectral class and with the value predicted from IRFM (Castelli, Gratton, & Kurucz 1997).

3. THE DATA

3.1. *Additional Sources of Data*

In order to estimate properly bolometric fluxes for the stars observed, broadband photometry is needed, particularly in the near- to mid-IR, where these stars emit much of their light. Magnitudes at 2.2 mm for the stars observed were found in Gezari et al. (1996). The 12 mm fluxes available for our targets from the *IRAS* Point Source Catalog (1987) were used as magnitudes, as described in Hickman, Sloan, & Canterna (1995): $[12] = -2.5 \log (f_{12\,\mu\rm m}/28.3\ \rm Jy)$. Reddening corrections were based upon the empirical reddening determination described by Mathis (1980). As discussed in Paper I, this determination differs little from van de Hulst's theoretical reddening curve number 15 (see Johnson 1968). The effects of reddening are small, given that the majority of bolometric flux contribution comes from relatively unaffected bandpasses, and given the proximity of the majority of the objects observed (<200 pc)—at 2.2 μm, a source at 200 pc will typically have $A_K = 0.04$. Monochromatic flux densities at each wavelength were obtained from the magnitudes using absolute calibrations by Hayes & Latham (1975), Hayes (1984), and Blackwell et al. (1983). Bolometric flux densities were generally computed from a simple numerical integration of the observed monochromatic flux densities from 0.45 to 12 μm, as found in the SIMBAD database. Flux contributions beyond 12 μm were estimated by integrating a Rayleigh-Jeans distribution, normalized to the 12 μm flux density. For stars with extensive dusty mass loss (e.g., late-M type), this is not entirely accurate; however, for these objects, the contribution to the overall flux longward of 12 μm is generally much less than 1%. Errors in the bolometric flux were estimated directly from the contribution of the photometric errors for each data point for a given star; average error in the determination of the bolometric flux was 18%. This compares favorably with the similar technique employed in Papers I and II, where the $F_{\rm tot}$ error was merely assumed to be 15% for all stars. The photometry values are listed in Table 5, and the derived bolometric flux values can be seen in Table 6, in addition to the other derived stellar parameters.

We have been careful to choose stars that are classified on the MK system, preferring spectral types estimated by Morgan or Keenan and their coworkers. Second choices have been spectral types from Hoffleit & Jaschek (1991) and Eggen (1960, 1967, 1976, 1992), which correlate very well with the Keenan types. In some cases, alternative sources were necessary; references in Table 5 indicate the origin of each star's spectral typing.

Last, angular size data available in Papers I and II have been utilized in this manuscript for two specific reasons. First, the data represent an independent body of interferometric data, taken at a separate instrument and processed with different data reduction software. The consistency of the results between the two interferometers is evidence for the soundness of the technique employed in this paper, as well as Papers I and II. Second, increasing the sample with inclusion of IOTA data allows us to extend our results over a larger range of spectral classes and colors.

3.2. *Temperature and Radius*

In deriving values for temperature and radius from the PTI observations, it is important to keep in mind that these quantities derive from angular sizes measured in the K band. This particular bandpass offers a number of advantages. First, it is well known that many stars—particularly those of the latest spectral types—exhibit evidence of circumstellar dust shells. This dust can be difficult to separate from the photosphere, which makes photospheric diameter determinations difficult, as pointed out by Tsuji (1978). The near-infrared avoids both the scatter of optical wavelengths as well as the thermal reradiation at longer infrared bandpasses, which penetrates to the stellar photosphere. Second, as discussed below, the effects of limb darkening in the near-infrared are minimized relative to shorter wavelengths. Third, angular sizes at these wavelengths are easily compared to those measured in previous investigations.

Stellar effective temperature, $T_{\rm eff}$, is defined in terms of the star's luminosity and radius by $L = 4\pi\sigma R^2 T_{\rm eff}^4$.

TABLE 5

SPECTRAL TYPE, PHOTOMETRY: V, $V-K$, $K-[12]$

Name	Other Names	HD	Spectral Type	Spectral Type (BSC5)	Spectral Type References	V	$V-K$	$K-[12]$
HR 79		1632	K5 III	K5 III	1	5.79	3.99	0.56
HR 259		5316	M4 III	M4 IIIab	1, 2, 3	6.20	5.19	0.56
HR 274	68 Psc	5575	G6 III	gG6	4	5.42	2.49	0.35
HR 351	84 Psc, χ Psc	7087	G8.5 III	G8.5 III–IIIa	5	4.66	2.30	0.47
HR 389	91 Psc	8126	K5 III	gK5	4	5.23	3.30	0.45
HR 450		9640	M2 III	M2 IIIab	2	5.89	4.04	0.55
HR 564		11928	M2 III	M2 III	2	5.82	4.39	0.55
HR 631	15 Ari	13325	M3 III	M3 IIIab	2	5.75	4.86	0.61
HR 736	14 Tri	15656	K5 III	K5 III	6, 7	5.15	3.49	0.57
HR 882	24 Per	18449	K2 III	K2 III	6, 7	4.94	2.85	0.51
HR 1343	54 Per	27348	G8 III	G8 III	5	4.93	2.17	
HR 1409	74 Tau, ϵ Tau	28305	G9.5 III	G9.5 IIICN0.5	5	3.55	2.20	0.50
HR 1533		30504	K3.5 III	K3.5 IIIBa0.2:	5	4.87	3.41	0.57
HR 1551	2 Aur	30834	K2.5 III	K2.5 IIIbBa0.4	5	4.77	3.29	0.63
HR 1739	109 Tau	34559	G8 III	G8 III	4	4.88	1.99	0.54
HR 1791	112 Tau, β Tau	35497	B7 III	B7 III	8	1.64	−0.41	
HR 1995	29 Aur, τ Aur	38656	G8 III	G8 IIIFe-1	5	4.53	2.19	
HR 2012	32 Aur, ν Aur	39003	K0 III	G9.5 III*	5	3.97	2.46	0.55
HR 2189		42471	M2 III	M2 IIIa	2	5.78	4.31	0.57
HR 2219	44 Aur, κ Aur	43039	G9 III	G8.5 IIIb	5	4.35	2.41	0.62
HR 2630	42 Gem, ω Gem	52497	G5 I	G5 IIa–Ib	9	5.18	2.19	0.39
HR 2696	63 Aur	54716	K3.5 III	K4 III–IIIa	5	4.89	3.38	0.50
HR 2805	66 Aur	57669	K1 IIIaFe-1	K1+ IIIaCN1	5	5.19	2.70	0.54
HR 5215		120819	M2 III	M2 III	2	5.87	4.18	0.43
HR 5429	25 Boo, ρ Boo	127665	K3 III	K3− III	5	3.57	2.91	0.56
HR 5510		130084	M1 III	M1 IIIb	2	6.28	4.25	0.47
HR 5638	46 Boo	134320	K2 III	gK2	10	5.67	3.00	0.49
HR 5681	49 Boo, δ Boo	135722	G8 III	G8 IIIFe-1	5	3.50	2.28	0.49
HR 5709	o CrB	136512	K0 III	K0 III	7	5.51	2.38	0.51
HR 5745		137853	M1 III	gM1	2	6.02	4.20	0.50
HR 6107	20 CrB, ν^1 CrB	147749	M2 III	M2 IIIab	3	5.20	4.35	0.54
HR 6208	IRC +20304	150580	K3	K2	11	6.06	3.12	0.51
HR 6258	50 Her	152173	M1 III	M1 IIIa	2	5.72	3.98	0.55
HR 6584		160677	M2 III	M2 IIIab	2	6.03	4.20	0.55
HR 6695	91 Her, θ Her	163770	K1 II	K1 IIaCN+2	5	3.87	2.84	0.56
HR 6820	IRC +20353	167193	K4 III	K4 III	7	6.12	3.49	0.54
HR 7237		177808	M0 III	M0 III	3	5.54	3.71	0.45
HR 7238		177809	M2.5 III	M2.5 IIIab	2	6.06	4.33	0.49
HR 7517	IRC +40361	186675	G7 III	G7+ III	7	4.89	2.16	0.47
HR 7759		193092	K3 IIIaFe-1	K3.5 IIab–IIb	5	5.24	3.79	0.46
HR 7806	39 Cyg	194317	K2.5 III	K2.5 IIIFe-0.5	5	4.44	3.00	0.58
HR 7834	41 Cyg	195295	F5 II	F5 II	12	4.02	1.05	0.54
HR 7847	44 Cyg	195593	F5 I	F5 Iab	12, 13	6.17	2.63	
HR 7942	52 Cyg	197912	K0 III	G9.5 III	5	4.23	2.36	
HR 7995	31 Vul	198809	G7 III	G7 IIIFe-1	5	4.61	1.64	0.80
HR 8008	32 Vul	199169	K4 III	K4 III	6, 7	4.99	3.37	0.48
HR 8044		200044	M3 III	M3 IIIab	2	5.65	4.44	0.50
HR 8306		206749	M2 III	M2 IIIab	5	5.49	4.18	0.60
HR 8555	IRC +30493	212988	K3	K2	11	5.98	3.36	0.56
HR 8684	48 Peg, μ Peg	216131	G8 III	G8+ III	5	3.48	2.05	0.52
HR 8796	56 Peg	218356	K0.5 II	G8 Ib	5	4.77	2.98	0.57
HR 8930	14 And	221345	K0 III	K0 III	14	5.22	2.49	0.53
HR 8942		221662	M3 III	M3 III	2	6.06	5.07	0.59
HR 8953		221905	M1 III	M1 III	2	6.45	4.59	
HR 9035		223755	M2.5 III	M2 III	2	6.11	4.10	0.63
HR 9055		224303	M2 III	M2 III	2	6.15	4.19	0.58
IRC +20092......		30354	M2 III		15	8.40	6.28	0.71
IRC +30086......		27796	M3 III		15	7.80	5.67	0.70
IRC +30105......		33463	M2 III?			6.38	4.79	0.60
IRC +30115......		35601	M1.5 I		5	7.35	5.61	0.92
IRC +30309......	V959 Her	159968	M1 III		16	6.42	5.01	0.62
IRC +30412......		190788	M3 I		5	7.86	6.19	0.83
IRC +30438......	FG Vul		M5 II		17	9.35	7.02	0.80
IRC +30465......	V2142 Cyg	200043	M3 III		18	7.20	5.11	0.68
IRC +30468......		200546	M2 III		19	7.20	5.16	0.54
IRC +40018......		6262	M3 III		18	7.08	4.90	0.62
IRC +40022......	YZ Tri	9500	M4 III		18	7.00	5.13	0.51
IRC +40254......		124696	K5 III		10	6.90	4.05	0.50
IRC +40337......		177697	K5?			7.76	4.90	0.38

REFERENCES.—(1) Haggkvist & Oja 1987; (2) Eggen 1992; (3) Eggen 1967; (4) McWilliam 1990; (5) Keenan & McNeil 1989; (6) Roman 1952; (7) Griffin & Redman 1960; (8) Cowley 1972; (9) Keenan & McNeil 1976; (10) Sato & Kuji 1990; (11) Duflot et al. 1995; (12) Morgan & Roman 1950; (13) Bidelman 1957; (14) Keenan & Keller 1953; (15) Metreveli 1968; (16) Eggen 1976; (17) Walker 1958; (18) Moore & Paddock 1950; (19) Heard 1956.

TABLE 6

BOLOMETRIC FLUX, EFFECTIVE TEMPERATURE, DISTANCE, RADIUS

Name	θ_R (mas)	F_{bol} (10^{-8} ergs cm^{-2} s^{-1})	T_{eff} (K)	Distance (pc)	Radius (R_{Sun})
HR 79	2.51 ± 0.05	45.9 ± 3.9	3844 ± 90	200.0 ± 36.0	54.1 ± 9.8
HR 259	3.67 ± 0.10	59.1 ± 3.6	3388 ± 70	178.6 ± 25.5	70.5 ± 10.3
HR 274	2.80 ± 0.11	32.8 ± 3.9	3348 ± 120	217.4 ± 33.1	65.5 ± 10.3
HR 351	1.64 ± 0.07	59.6 ± 10.8	5087 ± 256	135.1 ± 12.8	23.8 ± 2.5
HR 389	2.22 ± 0.06	48.3 ± 4.3	4144 ± 108	105.3 ± 8.9	25.1 ± 2.2
HR 450	2.42 ± 0.05	41.8 ± 3.8	3825 ± 96	181.8 ± 23.1	47.4 ± 6.1
HR 564	2.96 ± 0.06	52.2 ± 3.5	3656 ± 72	147.1 ± 17.3	46.9 ± 5.6
HR 631	3.75 ± 0.11	79.1 ± 5.7	3605 ± 84	204.1 ± 37.5	82.4 ± 15.3
HR 736	2.60 ± 0.11	60.8 ± 5.3	4057 ± 124	120.5 ± 11.6	33.7 ± 3.6
HR 882	2.08 ± 0.07	55.1 ± 8.8	4416 ± 192	107.5 ± 9.2	24.1 ± 2.2
HR 1343	1.44 ± 0.13	39.1 ± 5.9	4878 ± 290	69.4 ± 3.9	10.8 ± 1.2
HR 1409	2.57 ± 0.06	140.0 ± 30.5	5027 ± 280	47.6 ± 1.8	13.1 ± 0.6
HR 1533	2.93 ± 0.08	78.3 ± 7.3	4067 ± 111	161.3 ± 20.8	50.9 ± 6.7
HR 1551	2.79 ± 0.06	87.8 ± 14.5	4290 ± 183	172.4 ± 23.8	51.8 ± 7.2
HR 1739	1.42 ± 0.13	38.3 ± 8.8	4887 ± 362	63.3 ± 3.6	9.7 ± 1.1
HR 1791	1.59 ± 0.11	2593.5 ± 1139.0	13231 ± 1526	40.2 ± 1.5	6.9 ± 0.5
HR 1995	1.97 ± 0.08	58.8 ± 16.8	4616 ± 344	65.4 ± 3.4	13.9 ± 0.9
HR 2012	2.79 ± 0.06	105.9 ± 30.6	4496 ± 329	65.9 ± 3.8	19.8 ± 1.2
HR 2189	2.94 ± 0.06	70.5 ± 14.3	3954 ± 205		
HR 2219	2.16 ± 0.09	73.0 ± 16.1	4660 ± 276	51.8 ± 2.1	12.0 ± 0.7
HR 2630	1.50 ± 0.21	44.4 ± 29.5	4931 ± 892		
HR 2696	2.92 ± 0.10	72.4 ± 6.2	3995 ± 110	142.9 ± 18.4	44.9 ± 6.0
HR 2805	1.94 ± 0.17	46.0 ± 8.9	4375 ± 289	222.2 ± 49.4	46.4 ± 11.1
HR 5215	2.50 ± 0.05	44.6 ± 3.4	3823 ± 83	208.3 ± 30.4	56.1 ± 8.3
HR 5429	3.80 ± 0.12	187.1 ± 36.4	4440 ± 228	45.7 ± 1.7	18.7 ± 0.9
HR 5510	2.07 ± 0.05	35.3 ± 3.4	3962 ± 108		
HR 5638	1.44 ± 0.06	29.2 ± 2.4	4532 ± 135	128.2 ± 13.1	19.9 ± 2.2
HR 5681	2.71 ± 0.06	151.9 ± 30.5	4994 ± 257	35.8 ± 0.8	10.4 ± 0.3
HR 5709	1.18 ± 0.07	23.6 ± 4.4	4757 ± 265	84.0 ± 4.9	10.6 ± 0.9
HR 5745	2.42 ± 0.05	42.2 ± 3.3	3833 ± 85	238.1 ± 45.4	62.1 ± 11.9
HR 6107	3.68 ± 0.10	90.4 ± 12.1	3764 ± 136	169.5 ± 17.2	67.1 ± 7.1
HR 6208	1.24 ± 0.06	21.9 ± 1.6	4555 ± 139	137.0 ± 13.1	18.2 ± 2.0
HR 6258	2.32 ± 0.06	52.4 ± 5.6	4134 ± 124	285.7 ± 57.1	71.3 ± 14.4
HR 6584	2.26 ± 0.05	39.8 ± 2.5	3911 ± 76	163.9 ± 16.1	39.8 ± 4.0
HR 6695	3.07 ± 0.07	160.8 ± 52.8	4761 ± 395	204.1 ± 20.8	67.3 ± 7.0
HR 6820	1.54 ± 0.06	22.0 ± 1.2	4080 ± 99		
HR 7237	2.27 ± 0.05	47.2 ± 3.4	4075 ± 86	185.2 ± 20.6	45.2 ± 5.1
HR 7238	2.40 ± 0.05	42.6 ± 2.9	3859 ± 78	227.3 ± 31.0	58.7 ± 8.1
HR 7517	1.18 ± 0.06	42.1 ± 5.4	5502 ± 228	85.5 ± 3.7	10.8 ± 0.7
HR 7759	1.19 ± 0.06	74.7 ± 4.7	6321 ± 191	303.0 ± 45.9	38.7 ± 6.2
HR 7806	2.99 ± 0.08	92.2 ± 20.4	4192 ± 239	78.1 ± 3.7	25.2 ± 1.4
HR 7834	1.43 ± 0.08	95.5 ± 33.5	6118 ± 564	232.6 ± 27.0	35.8 ± 4.6
HR 7847	1.23 ± 0.14	22.3 ± 11.6	4595 ± 656		
HR 7942	2.35 ± 0.05	84.2 ± 38.5	4626 ± 531	63.3 ± 2.4	16.0 ± 0.7
HR 7995	1.54 ± 0.29	51.2 ± 14.2	5040 ± 583	66.2 ± 2.6	11.0 ± 2.1
HR 8008	2.46 ± 0.05	70.6 ± 6.8	4324 ± 113	227.3 ± 36.2	60.2 ± 9.7
HR 8044	3.33 ± 0.08	63.1 ± 4.4	3615 ± 77	181.8 ± 26.4	65.2 ± 9.6
HR 8306	3.24 ± 0.07	66.7 ± 5.0	3717 ± 80	181.8 ± 19.8	63.4 ± 7.1
HR 8555	1.52 ± 0.06	31.9 ± 2.4	4507 ± 123	285.7 ± 57.1	46.8 ± 9.6
HR 8684	2.60 ± 0.06	142.1 ± 47.5	5017 ± 424	35.8 ± 1.0	10.0 ± 0.4
HR 8796	2.27 ± 0.05	72.5 ± 7.6	4535 ± 129	163.9 ± 18.8	40.0 ± 4.7
HR 8930	1.79 ± 0.07	33.3 ± 4.5	4206 ± 165	76.3 ± 4.1	14.7 ± 1.0
HR 8942	3.70 ± 0.10	71.7 ± 7.4	3542 ± 103		
HR 8953	2.53 ± 0.05	49.3 ± 28.0	3896 ± 554		
HR 9035	2.46 ± 0.05	36.3 ± 3.2	3660 ± 88	166.7 ± 22.2	44.2 ± 6.0
HR 9055	2.41 ± 0.05	36.5 ± 2.8	3704 ± 80	185.2 ± 27.4	48.1 ± 7.2
IRC +20092	2.41 ± 0.07	30.6 ± 6.3	3545 ± 191		
IRC +30086	2.41 ± 0.05	18.2 ± 1.1	3111 ± 56		
IRC +30105	2.87 ± 0.06	47.3 ± 6.1	3623 ± 122		
IRC +30115	3.11 ± 0.07	29.0 ± 2.4	3082 ± 73		
IRC +30309	2.95 ± 0.06	49.5 ± 4.1	3613 ± 84		
IRC +30412	2.91 ± 0.06	33.1 ± 3.7	3291 ± 98		
IRC +30438	2.54 ± 0.06	11.0 ± 1.2	2673 ± 80		
IRC +30465	2.21 ± 0.05	27.1 ± 1.5	3595 ± 66	294.1 ± 60.6	69.9 ± 14.5
IRC +30468	2.14 ± 0.05	25.1 ± 1.9	3585 ± 79	263.2 ± 55.4	60.5 ± 12.8
IRC +40018	2.39 ± 0.09	27.9 ± 4.6	3480 ± 157		
IRC +40022	2.49 ± 0.05	35.9 ± 6.7	3629 ± 174		
IRC +40254	1.57 ± 0.07	18.2 ± 1.8	3855 ± 129	303.0 ± 73.5	51.3 ± 12.7
IRC +40337	1.34 ± 0.06	18.5 ± 5.0	4194 ± 298		

Rewriting this equation in terms of angular diameter θ_R and bolometric flux $F_{\rm tot}$, $T_{\rm eff}$ can be expressed as $T_{\rm eff} = 2341(F_{\rm tot}/\theta_R^2)^{1/4}$; the units of $F_{\rm tot}$ are 10^{-8} ergs cm^{-2} s^{-1}, and $\theta_{\rm R}$ is in mas. The angular size utilized here is the Rosseland angular diameter, which corresponds to the surface where the Rosseland mean optical depth equals unity. As advocated by Scholz & Takeda (1987), this is the most appropriate surface for computing an effective temperature; utilizing the same evaluation of Scholz & Takeda's model atmospheres found in Papers I and II, we calculate the relationship $\theta_{\rm R} \approx 1.022\theta_{\rm UD}$ in the K band. Thus, in the infrared this effect is well contained within the errors of this investigation but is included for completeness. The effect is larger at other wavelength bands (see van Belle et al. 1996 for a discussion).

Stellar radius is given by $R = 0.1076\theta_{\rm R}\, d$; the units of R are $R_{\rm Sun}$, d is in parsecs, and $\theta_{\rm R}$ is the Rosseland diameter. Distances were obtained from the parallaxes of *Hipparcos* (Perryman et al. 1997); distances (and associated radii) with errors in excess of 25% were discarded from the analyses in the next section. The derived temperature and radius values are listed in Table 6.

4. EMPIRICAL RELATIONSHIPS FOR GIANT STARS

4.1. *Spectral Type*

The effective temperature scale as a function of spectral type of K and M giants is well studied (Ridgway et al. 1980; Di Benedetto & Rabbia 1987; Paper I; Paper II). As a check of our results, it is worthwhile to compare the effective temperature scale obtained in this study to that of Paper II. The fit from Paper II is $T_{\rm eff} = -106 \times {\rm ST} + 4580$ K, where ST $= -2, \ldots 0, \ldots 5, 6, \ldots 14$ corresponding to spectral classes G8, …, K0, …, K5, M0, …, M8. Comparing the PTI data to this fit, we find that average absolute difference to be 120 K, and the average difference is less than 10 K; comparing the average absolute difference to the average rms spread of each bin, we find that the mean is less than half of a standard deviation for the PTI data, which is good agreement. A fit of the composite data set gives

$$T_{\rm eff} = -109 \times {\rm ST} + 4570 \text{ K} ,$$

with a reduced χ^2 of 3.7. This fit is statistically identical to the one given in Paper II, although it is marginally cooler for the later spectral types (~ 60 K for M7 III). By spectral type bin, the average standard deviation of the temperatures is $\Delta T_{\rm rms} \approx 270$ K.

Comparison of these results to those found in Paper II leads to a consideration of the relative sample between the two interferometers. It is reasonable to expect that this is due to either a slight bias in either the IOTA sample to cooler, larger stars, or, conversely, to one in the PTI sample toward either hotter, smaller stars or more distant cool stars. For the more distant stars observed by PTI, these objects tend to be fainter and less well studied; in particular, the spectral types are potentially poorer, as are the extinction corrections. As such, the standard error of ± 270 K is larger than that found in Paper II, which was ± 192 K. The mean relative error in angular diameter is $\sigma_\theta/\theta \approx 0.039$, which leads to an error contribution of ± 1.9%. For a star of 3000 K, this corresponds to ± 60 K. The mean bolometric flux relative error was 17%, which leads to an error contribution of 4.25%, which is approximately ± 130 K. The remainder of the error is presumably contributed to by improper spectral typing; errors of roughly two subtypes would drive the standard error to ~ 260 K, which is roughly the observed value.

Given the large data set for the giant stars and the recent release of the *Hipparcos* data (Perryman et al. 1997), we also draw some general conclusions about the dependence of linear radii upon spectral subtype. A weighted exponential fit to the data results in the following relationship:

$$R = 4.04 + 9.58 \times 10^{0.096 \times {\rm ST}}\ R_{\rm Sun} ,$$

with a reduced χ^2 of 8.7 (noting that a *linear* fit to the data results in a reduced χ^2 of 17.8). The poor χ^2 is a shortcoming of the fit owing to the scaling of error bars with star size owing to the primary error source being parallactic error; as such, the earlier spectral types are potentially a better fit, at the expense of the later spectral type.

Given the poor χ^2, a better predictor of radius as a function of spectral type is actually average values by spectral type bin, which is not affected by the scaling of radius errors for the larger stars. The sizes predicted by the bins tend to be slightly (~ 35%) larger than comparable numbers expected from Paper I. This is consistent with the result that the space-based *Hipparcos* parallax numbers tended to indicate distances greater than expected from ground-based parallaxes, which were all that were available at the time of Paper I's writing. However, we are in agreement with the observation from Paper I that a factor of 2 increase in size accompanies every 500 K decrease in effective temperature. Examining the means and standard deviations by spectral type bin, we see that on average the standard deviations are 50% of the mean values, indicating the limitations of spectral type–inferred sizes. A more robust inference is derived from $V-K$ color (§ 4.2). Comparing to sizes as estimated from Dumm & Schild (1998), the mean size by spectral type bin agrees quite well; on average, our sizes are 98% of the sizes given by Dumm & Schild. There is some overlap in the data sets in this paper and that of Dumm & Schild, in that the authors utilized some angular diameters from Paper I in their analysis (among others); however, the agreement is still quite significant given the disparate methods and inhomogeneous data sets. The spectral type–dependent data and resultant fits may be seen in Figure 1 and Table 7.

4.2. *$V-K$ Color, $K-[12]$ Color*

Given the potential of misclassifications even when being selective about sources of spectral typing, a second parameter used in investigating the potential dependencies of stellar temperature and size was giant star color, as characterized by both $V-K$ and $K-[12]$. An interesting additional comparison that can be drawn for both of these colors is the departure of the observed stars' temperatures from nominal blackbody behavior, as blackbody temperatures can be well determined from the Planck function for any given value of $V-K$ or $K-[12]$.

$V-K$ Color.—A numerical comparison of the agreement of the IOTA and PTI data sets was not readily possible using fits given the rather separate sample space of the two data sets ($2 < V-K_{\rm PTI} < 5$, while $3 < V-K_{\rm IOTA} < 9$) and the exponential nature of the empirical function. However, by inspection, the region of overlap is in good agreement, and the resultant fit to the composite data set greatly benefited from the wide coverage of the data points. The exact form is

$$T_{\rm eff} = 3030 + 4750 \times 10^{-0.187(V-K)} \text{ K} ,$$

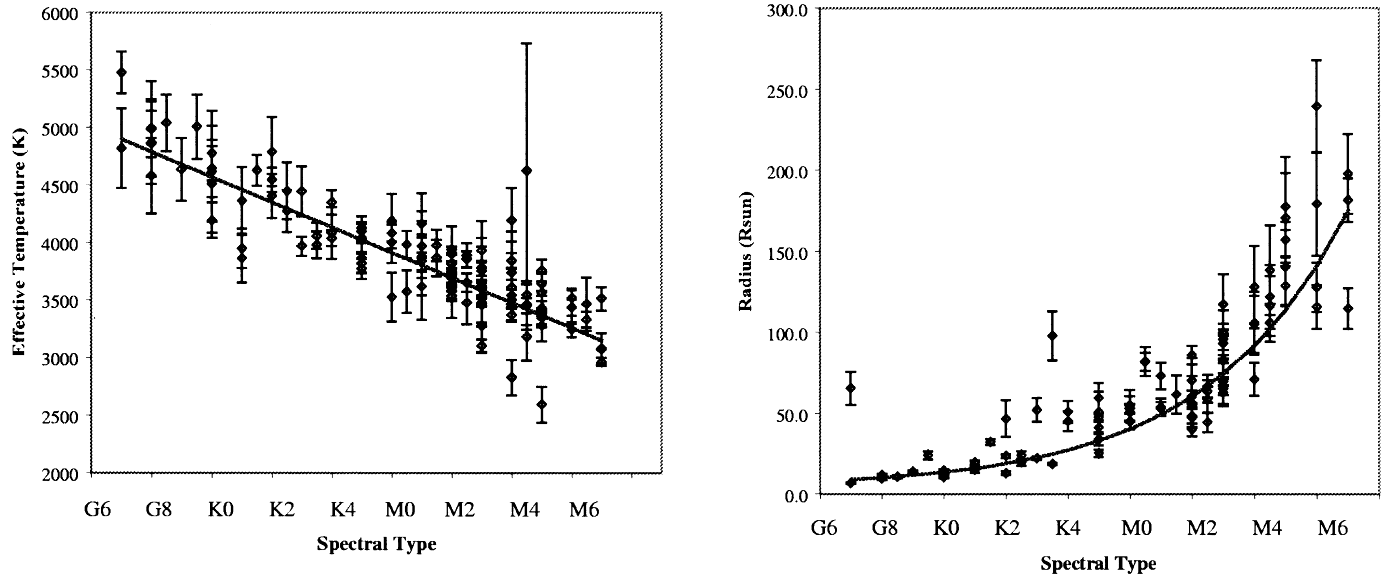

FIG. 1.—Temperature and radius as a function of spectral type. Data from this paper are plotted for luminosity class III stars; in addition, temperatures and radii derived (Dyck et al. 1996, 1998) are plotted in all the figures.

with a reduced χ^2 of 3.0. A plot of the data, the fit, and the corresponding blackbody curve can be seen in Figure 2 (*left*). In Table 8, binned averages and fits for the temperature data are presented for bins ranging from 2.0 to 9.0, in addition to the corresponding numbers for the radius data. One of the most striking features of Figure 2 (*left*) is the departure of the temperature data points from expected blackbody behavior. This is reflected in Table 8, where all of the mean temperatures deviate from blackbody temperatures by 3 standard deviations or more for $V-K = 6.0$.

Comparing this $T_{\rm eff}$ versus $V-K$ calibration to the previous one of Di Benedetto (1993), the IOTA/PTI calibration is systematically hotter in the $V-K = 3.0$–5.0 range for both the fit and the measured data by up to 200 K (at $V-K$ of 3.78). We suspect this is indicative of two linear fits in the Di Benedetto paper that "bend" at $\sim$3.75. A similar fit to our data indicated an unchanged reduced χ^2 of 3.0 with the additional degree of freedom being used. As such, we believe the fit presented herein is more appropriate.

A similar exercise exploring the linear radius data as a function of $V-K$ color delivers the following function:

$$R = 1.76 \times (V-K)^{2.36}\ R_{\rm Sun}\ ,$$

with a reduced χ^2 of 7.3. As with the linear radius–spectral type fit, this particular function has a poor χ^2, and the mean radius values seen in the $V-K$ bins are a better indicator of

TABLE 7

EFFECTIVE TEMPERATURE, LINEAR RADII AS A FUNCTION OF SPECTRAL TYPE: OBSERVED DATA AND FITS

Spectral Type	N_T	$T_{\rm eff} \pm$ Weighted Error	Standard Deviation	$T_{\rm fit}$	N_R	$R_{\rm avg} \pm$ Weighted Error	Standard Deviation	$R_{\rm fit}$
G7	2	5335 ± 161	533	4897	2	11.3 ± 0.4	0.8	9.0
G8	6	4910 ± 122	169	4788	6	10.6 ± 0.2	6.3	10.2
G9	3	4903 ± 152	224	4679	3	13.1 ± 0.4	7.9	11.7
K0	6	4513 ± 99	298	4569	6	13.9 ± 0.3	3.4	13.6
K1	4	4280 ± 90	369	4460	4	23.9 ± 0.9	14.9	16.0
K2	6	4520 ± 66	181	4351	6	20.8 ± 0.6	14.6	19.0
K3	6	4065 ± 52	266	4241	6	20.5 ± 0.6	22.6	22.7
K4	5	4094 ± 46	144	4132	4	45.0 ± 2.7	9.3	27.3
K5	6	3950 ± 39	152	4023	6	38.8 ± 1.3	13.4	33.1
M0...........	6	3985 ± 53	293	3914	6	59.1 ± 2.3	17.7	40.3
M1...........	10	3858 ± 37	178	3804	6	62.6 ± 2.5	13.3	49.3
M2...........	17	3750 ± 22	150	3695	13	57.8 ± 1.8	23.6	60.5
M3...........	17	3573 ± 22	222	3586	14	71.5 ± 2.5	27.2	74.5
M4...........	13	3425 ± 37	482	3476	8	105.5 ± 5.3	25.0	92.0
M5...........	14	3424 ± 30	431	3367	9	139.6 ± 5.6	44.7	113.8
M6...........	6	3375 ± 34	106	3258	4	147.9 ± 7.7	41.1	141.0
M7...........	6	3095 ± 29	279	3149	3	131.9 ± 11.7	109.9	175.0
M8...........	0			3039	0			217.5

NOTE.—Observed data are the values derived in this paper and in Dyck et al. 1996, 1998. Error bars are standard deviations by spectral type. N_T and N_R represent the number of data points for each spectral type bin for effective temperature and radius analyses, respectively. The mean standard deviation of $T_{\rm eff}$ is 7% of the weighted average for each of the spectral type bins, while the mean weighted error is 1.5%; the mean standard deviation and weighted error for $R_{\rm avg}$ are 50% and 3.5%, respectively. $T_{\rm fit}$ and $R_{\rm fit}$ are the results of weighted χ^2 minimizations to the temperature data for stars in spectral classes G7 through M8. $\chi^2(T_{\rm fit}) = 3.72$, $\chi^2(R_{\rm fit}) = 8.66$. The average standard deviation of $T_{\rm eff}$ is 270 K and represents the accuracy of $T_{\rm fit}$; the corresponding number for $R_{\rm fit}$ is the average standard deviation size of 50%.

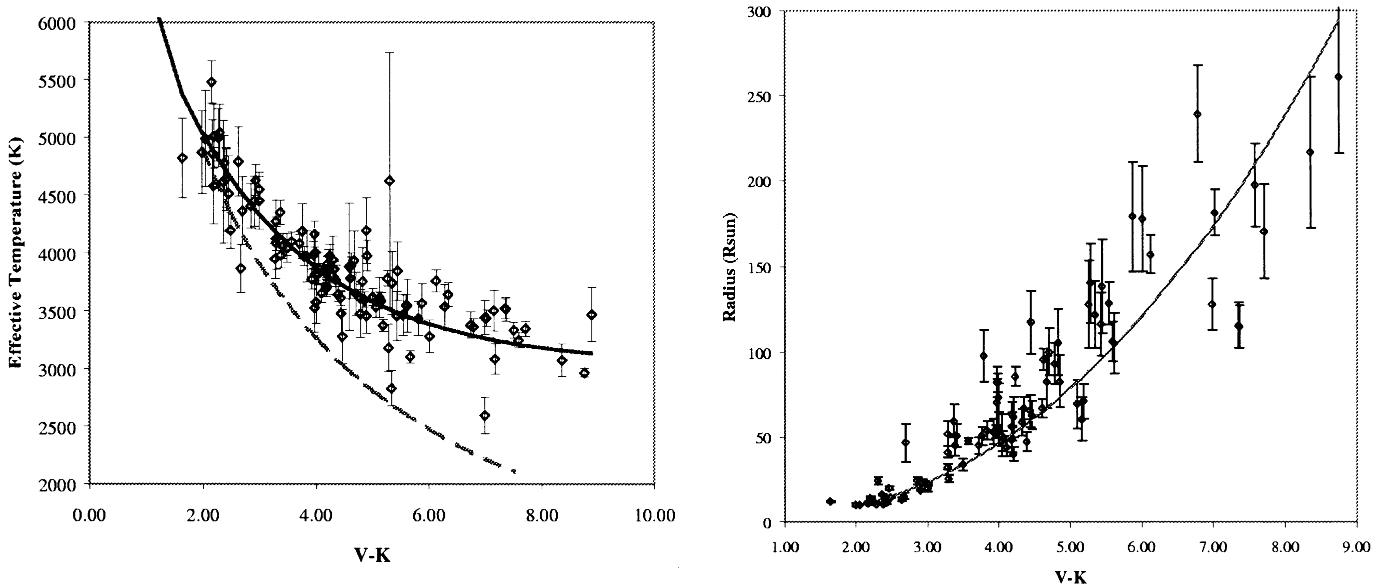

FIG. 2.—Effective temperature and radius as a function of $V-K$ color for luminosity class III stars. The strong departure from blackbody behavior (*dotted line*) at $V-K = 6.0$ is indicated to be statistically significant by the data at the 3 σ level.

the expected relationship between $V-K$ and radius. Examining the means and standard deviations by spectral type bin, we see that on average the standard deviations are 30% of the mean values. A plot of the stellar radii as a function of $V-K$ can be seen in Figure 2 (*right*).

An exclusion from both of the $V-K$ fits is HR 274. This particular object has an unusually low temperature and large size for both its spectral classification (G6 III) and $V-K$ color (2.49). Given that this particular object was observed on only one night, the possibility exists for either an anomalous measurement or an unexpected secondary companion; further observations of this object during the upcoming observing season are expected to resolve the source of the anomaly.

$K-[12]$ Color.—Neither linear nor exponential fits of temperature or radius as a function of $K-[12]$ color were statistically significant. However, as with the behavior seen for the $V-K$ data, one of the most striking features of the temperature versus $K-[12]$ plot is the departure of the temperature data points from expected blackbody behavior. This is reflected in Table 9, where all of the mean temperatures deviate from blackbody temperatures by 2.5 standard deviations or more for $K-[12] = 0.80$. A general trend of stellar radii toward larger values ($R > 100\,R_{\mathrm{Sun}}$) are seen for $K-[12] = 0.80$ as well. Both the temperature and radius plots can be seen in Figure 3; temperature averages and standard deviations are listed in the table for bins from $0.35 < K-[12] < 1.80$.

TABLE 8

EFFECTIVE TEMPERATURE, LINEAR RADII AS A FUNCTION OF $V-K$ COLOR: OBSERVED DATA, FITS, AND TEMPERATURE EXPECTATIONS FOR A BLACKBODY RADIATOR

$V-K$ Bin	Bin Size	N_T	$T_{\mathrm{eff}} \pm$ Weighted Error	Standard Deviation	T_{fit}	T_{bbr}	N_R	$R_{\mathrm{avg}} \pm$ Weighted Error	Standard Deviation	R_{fit}
2.0	0.5	6	5101 ± 113	331	5036	4899	6	11.0 ± 0.2	1.8	9.0
2.5	0.5	11	4504 ± 74	355	4647	4343	11	11.6 ± 0.2	12.3	15.3
3.0	0.5	5	4533 ± 69	100	4333	3908	5	20.6 ± 0.5	2.8	23.5
3.5	0.5	11	4093 ± 31	118	4081	3558	10	37.8 ± 1.0	11.9	33.8
4.0	0.5	20	3833 ± 22	175	3877	3268	19	57.2 ± 1.5	16.7	46.3
4.5	0.5	13	3739 ± 30	206	3713	3025	10	68.7 ± 2.5	23.3	61.2
5.0	0.5	13	3558 ± 25	238	3580	2816	6	77.5 ± 5.4	17.1	78.4
5.5	0.5	11	3384 ± 34	502	3474	2636	8	118.9 ± 6.0	14.0	98.2
6.0	0.5	4	3566 ± 65	213	3388	2478	3	161.4 ± 9.9	17.2	120.5
6.5	0.5	3	3526 ± 71	133	3319	2339	0			145.6
7.0	0.5	6	3320 ± 42	359	3263	2215	3	166.8 ± 9.5	59.2	173.4
7.5	0.5	5	3364 ± 33	125	3218	2104	4	129.4 ± 8.2	47.5	204.0
8.0	1.0	4	3294 ± 37	136	3182	2003	3	190.3 ± 16.9	23.8	237.6
9.0	1.0	2	2978 ± 36	491	3129	1829	1			313.7

NOTE.—Observed data are the values derived in this paper and in Dyck et al. 1996, 1998. Error bars are weighted error by $V-K$ bin. N_T and N_R represent the number of data points for each spectral type bin for effective temperature and radius analyses, respectively. The mean standard deviation of T_{eff} is 7% of the weighted average for each of the $V-K$ bins, while the mean weighted error of T_{eff} is 1.3%; the mean standard deviation and weighted error for R_{avg} are 30% and 4.1%, respectively. T_{fit} and R_{fit} are the results of weighted χ^2 minimizations to the temperature data for stars with $1.75 < V-K < 9.0$. $\chi^2(T_{\mathrm{fit}}) = 2.99$, $\chi^2(R_{\mathrm{fit}}) = 7.26$. All of the T_{eff} values for $V-K = 6.0$ deviate from T_{bbr} by 3 standard deviations or more, with the exception of the $V-K = 9.0$ bin, where the sampling is insufficient. The average standard deviation of T_{eff} is 250 K and represents the accuracy of T_{fit}; the corresponding number for R_{fit} is the average standard deviation size of 30%.

TABLE 9

EFFECTIVE TEMPERATURE, LINEAR RADII AS A FUNCTION OF $K-[12]$ COLOR: OBSERVED DATA, FITS, AND TEMPERATURE EXPECTATIONS FOR A BLACKBODY RADIATOR

$K-[12]$ Bin	Bin Size	N_T	T_{eff} ± Weighted Error	Standard Deviation	T_{bbr}	N_R	R_{avg} ± Weighted Error	Standard Deviation
0.35	0.05	1			5454	1		
0.40	0.05	2	3723 ± 167	532	5076	1		
0.45	0.05	8	4081 ± 36	704	4741	7	12.7 ± 0.5	41.9
0.50	0.05	17	3990 ± 28	565	4453	16	11.2 ± 0.2	32.6
0.55	0.05	23	3785 ± 22	394	4205	21	19.1 ± 0.4	47.9
0.60	0.05	20	3676 ± 25	407	3981	15	18.9 ± 0.5	63.5
0.65	0.05	11	3744 ± 40	429	3784	11	33.1 ± 1.1	69.9
0.70	0.10	11	3514 ± 28	250	3608	6	92.7 ± 4.1	42.7
0.80	0.10	2	3810 ± 153	1040	3304	2	12.1 ± 0.6	167.1
0.90	0.10	3	3536 ± 70	83	3052	2	108.0 ± 9.6	11.1
1.00	0.20	4	3412 ± 45	151	2839	3	144.7 ± 9.1	44.9
1.20	0.30	2	3347 ± 49	19	2499	1		
1.50	0.30	3	3250 ± 53	154	2130	2	202.2 ± 21.5	15.1
1.80	0.30	3	2959 ± 35	442	1865	1		

NOTE.—Observed data are the values derived in this paper and in Dyck et al. 1996, 1998. Error bars are weighted error by $K-[12]$ bin. N_T and N_R represent the number of data points for each spectral type bin for effective temperature and radius analyses, respectively. The mean standard deviation of T_{eff} is 11% of the weighted average for each of the $K-[12]$ bins, while the mean weighted error of T_{eff} is 2%. All of the T_{eff} values for $K-[12] = 0.90$ deviate from T_{bbr} by 2.5 standard deviations or more.

An exclusion from both of the $K-[12]$ fits is HR 7995. This particular object has a temperature and radius consistent with its spectral classification (G7 III), although it appears to have an anomalously red $K-[12]$ color (0.80). Unlike HR 274 (see above), this object was observed on multiple nights, and there appears little room for questioning the angular size; we believe that our value obtained for the $K-[12]$ is the more likely source of error.

Departures from Blackbody Behavior.—Both the $V-K$ and $K-[12]$ data deviate from blackbody behavior at a stellar effective temperature of $T \approx 3500$ K; the shorter wavelength color shows a gradual departure from the BBR curve, while the longer wavelength color indicates a sharper turnoff. Several mechanisms are being explored as reasonable explanations for the deviation from the blackbody curves. Equivalent widths of absorption features in the K band, particularly $^{12}CO(2,0)$ at 2.29 μm, grow with decreasing temperature (Ramirez et al. 1997). However, there does not appear to be any sharp onset of this effect at 3500 K; indeed, the gradual appearance of this and other K-band absorption features begins at a much warmer temperature of 4600 K. Preliminary inspection of the visibilities from individual spectral channels available from PTI also show no evidence for specific features at the narrow bandpass channel that contains the $^{12}CO(2,0)$ feature. V-band absorption features, such as MgH and TiO, appear as likely candidates in depressing V relative to K for low temperatures (Barbuy, Erdelyi-Mendes, & Milone 1992; Jørgensen 1994). Given that both K and [12] are on the Rayleigh-Jeans tail of the Planck function, $K-[12]$ should

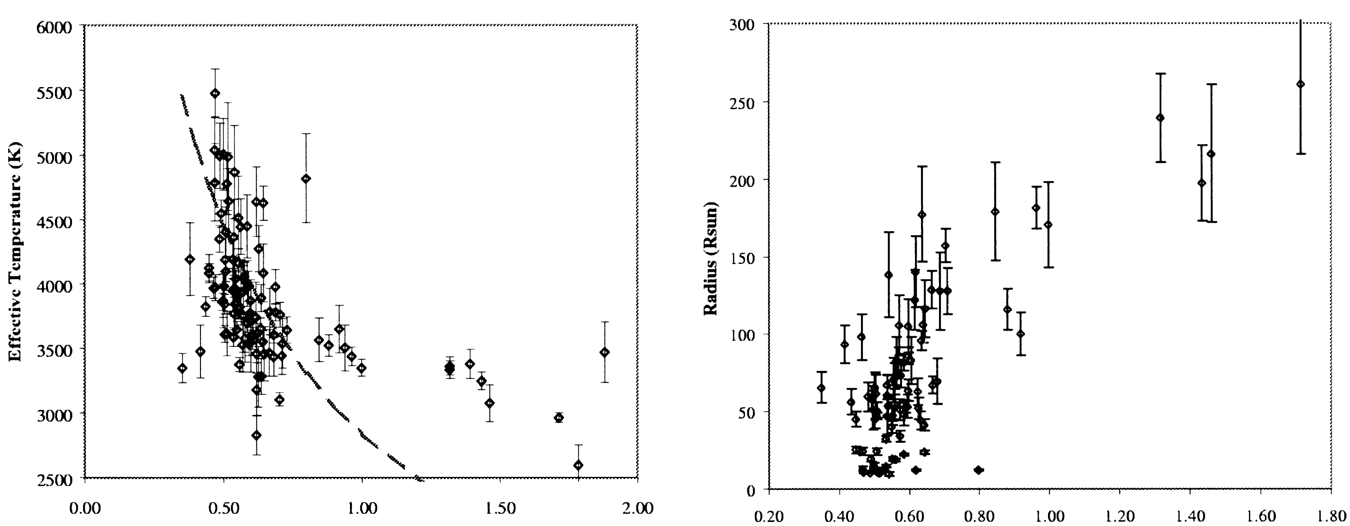

FIG. 3.—Effective temperature and radius as a function of $K-[12]$ color for luminosity class III stars. Note the strong departure from blackbody behavior at $K-[12] > 0.80$; it is statistically significant at the 2.5 σ level.

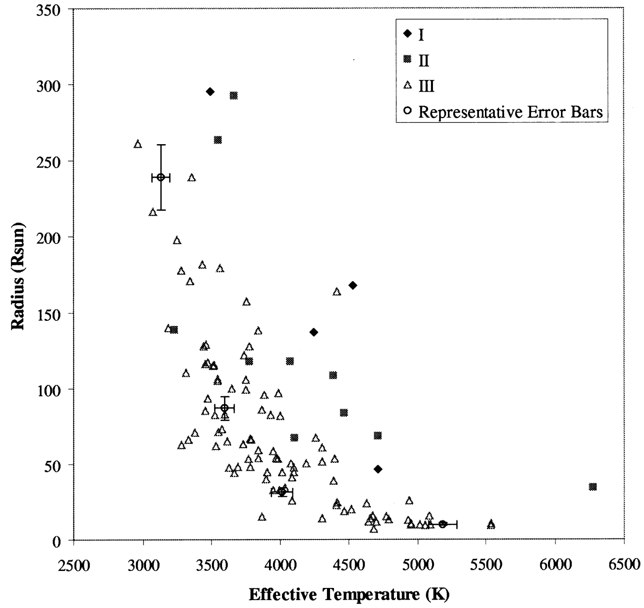

FIG. 4.—Radius as a function of effective temperature by luminosity class. Representative error bars are 4% for temperature and 18% for radius, from the data given in the paper. The luminosity class I and II objects are on average ∼3 times the radius of the giant stars for a given temperature.

be nearly constant for all of the stars plotted, unless there is perhaps some circumstellar material. Specifically, $K-[12]$ color is a reasonable indicator of mild dusty mass loss (Le Sidander & Le Bertre 1996), and the 12 μm excesses are quite consistent with rates between 10^{-10} $M_{\rm Sun}$ yr^{-1} (Le Sidander & Le Bertre) and 10^{-7} to 10^{-8} $M_{\rm Sun}$ yr^{-1} (Beichman et al. 1990); scattering of short-wavelength light by a dusty envelope would also produce the $V-K$ excess.

5. BRIGHT GIANTS AND SUPERGIANTS

As we previously observed in Paper II, a plot of the radius versus temperature for the luminosity class I, II, and III objects exhibited a tendency for the higher luminosity objects to have a greater radius at a given temperature. On average, the luminosity class I and II objects were ∼3 times larger than their giant star counterparts at a given temperature. A plot of the total data set for giants and supergiants can be seen in Figure 4.

Again, as with Paper II, the limitations in the available distance data are what preclude the construction of an H-R diagram from the data on hand. While the release of the *Hipparcos* data has greatly enabled the analyses of this paper with regard to stellar radii, the uncertainties of the parallax data still restrict the derivable luminosities.

6. CONCLUSION

Further parameterization of the fits to the stars in our observed sample has the potential to reduce the spread in those fits greatly, particularly those as a function of $V-K$ color. Specifically, characterization of surface gravity g in a manner independent of assumptions about a star's mass M can lead to determinations of M from g and linear radius. Preliminary research into this line of thinking appears to be quite promising and will be the subject of a forthcoming manuscript. Continuing observations at PTI will increase the size of our available database and will specifically concentrate upon luminosity class I and II objects, in addition to giant stars with spectral types earlier than G7.

We would like to thank Mel Dyck and Steve Ridgway for helpful remarks in preparing this manuscript. This research has made use of the SIMBAD and VizieR databases, operated by the CDS, Strasbourg, France. We gratefully thank the staffs of the Palomar Observatory and Whipple Observatory for their hospitality during our many stays. G. T. v. B. and B. T. were supported while students at the University of Wyoming by NASA grant NGT-40050 to the Wyoming Planetary and Space Science Center and would like to thank Ron Canterna for use of computer resources at UW. Portions of this work were performed at the Jet Propulsion Laboratory, California Institute of Technology under contract with NASA.

REFERENCES

Barbuy, B., Erdelyi-Mendes, M., & Milone, A. 1992, A&AS, 93, 235
Beichman, C. A., Chester, T., Gillett, F. C., Low, F. J., Matthews, K., & Neugebauer, G. 1990, AJ, 99, 1569
Bidelman, W. P. 1957, PASP, 69, 147
Blackwell, D. E., Leggett, S. K., Petford, A. D., Mountain, C. M., & Selby, M. J. 1983, MNRAS, 205, 897
Blackwell, D. E., & Lynas-Gray, A. E. 1994, A&A, 282, 899
Blackwell, D. E., Shallis, M. J., & Selby, M. J. 1979, MNRAS, 188, 847
Boden, A. F., et al. 1998, ApJ, 504, L39
Castelli, F., Gratton, R. G., & Kurucz, R. L. 1997, A&A, 318, 841
Colavita, M. M., et al. 1999, PASP, in press
Cowley, A. 1972, AJ, 77, 750
Cowley, A., Cowley, C., Jaschek, M., & Jaschek, C. 1969, AJ, 74, 375
Di Benedetto, G. P. 1993, A&A, 270, 315
Di Benedetto, G. P., & Rabbia, Y. 1987, A&A, 188, 114
Duflot, M., Figon, P., & Meyssonnier, M. 1995, A&AS, 114, 269
Dumm, T., & Schild, H. 1998, New Astron, 3, 137
Dyck, H. M., Benson, J. A., van Belle, G. T., & Ridgway, S. T. 1996, AJ, 111, 1705 (Paper I)
Dyck, H. M., van Belle, G. T., & Thompson, R. R. 1998, AJ, 116, 981 (Paper II)
Eggen, O. J. 1960, MNRAS, 120, 448
———. 1967, ApJS, 14, 307
———. 1976, PASP, 88, 426
———. 1992, AJ, 104, 27
Garrison, R. F., & Gray, R. O. 1994, AJ, 107, 1556
Gezari, D. Y., Pitts, P. S., Schmitz, M., & Mead, J. M. 1996, Catalog of Infrared Observations, Edition 3.5 (unpublished; available from VizieR)
Griffin, R. F., & Redman, R. O. 1960, MNRAS, 120, 287
Haggkvist, L., & Oja, T. 1987, A&AS, 68, 259.
Hayes, D. S. 1984, in Calibration of Fundamental Stellar Quantities, ed. D. S. Hayes, L. E. Pasinetti, & A. G. D. Philip (Dordrecht: Reidel), 246
Hayes, D. S., & Latham, D. W. 1975, ApJ, 197, 593
Heard, J. F. 1956, Publ. David Dunlap Obs., 2, 105
Hickman, M. A., Sloan, G. C., & Canterna, R. C. 1995, AJ, 110, 2910
Hoffleit, D., & Jaschek, C. 1991, The Bright Star Catalogue (5th ed.; New Haven: Yale Univ. Obs.)
Houk, N. 1995, IAU Circ. 6253.
Hutter, D. J., et al. 1989, ApJ, 340, 1103
IRAS Catalog of Point Sources, Version 2.0. 1987 (Washington, DC: GPO)
Johnson, H. L. 1968, in Stars and Stellar Systems, 7, Nebulae and Interstellar Matter, ed. B. M. Middlehurst & L. H. Aller (Chicago: Univ. of Chicago Press), chap. 5
Jørgensen, U. G. 1994, A&A, 284, 179
Keenan, P. C., & Keller, G. 1953, ApJ, 117, 241
Keenan, P. C., & McNeil, R. C. 1976, An Atlas of Spectra of the Cooler Stars: Types G, K, M, S, and C (Columbus: Ohio State Univ. Press)
———. 1989, ApJS, 71, 245
Le Sidaner, P., & Le Bertre, T. 1996, A&A, 314, 896
Mathis, J. S. 1980, ARA&A, 28, 37
McWilliam, A. 1990, ApJS, 74, 1075
Metreveli, M. D. 1968, Byull. Abastumanskaya Astrofiz. Obs., 38, 93
Moore, J. H., & Paddock, G. F. 1950, ApJ, 112, 48
Morgan, W. W., & Keenan, P. C. 1973, ARA&A, 11, 29
Morgan, W. W., & Roman, N. G. 1950, ApJ, 112, 362
Morgan, W. W., Whitford, A. E., & Code, A. D. 1953, ApJ, 118, 318
Mozurkewich, D., et al. 1991, AJ, 101, 2207

Noguchi, K. 1990, PASJ, 42, 419
Perrin, G., Coude Du Foresto, V., Ridgway, S. T., Mariotti, J.-M., & Benson, J. A. 1995, Proc. SPIE, 2476, 120
Perryman, M. A. C., et al. 1997, A&A, 323, L49
Ramirez, S. V., DePoy, D. L., Frogel, J. A., Sellgren, K., & Blum, R. D. 1997, AJ, 113, 1411
Richichi, A., Baffa, C., Calamai, G., & Lisi, F. 1996, AJ, 112, 2786
Ridgway, S. T., Jacoby, G. H., Joyce, R. R., & Wells, D. C. 1980, AJ, 85, 1496
Roman, N. G. 1952, ApJ, 116, 122
Sato, K., & Kuji, S. 1990, A&AS, 85, 1069
Scholz, M., & Takeda, Y. 1987, A&A 186, 200
Shao, M., Colavita, M. M., Hines, B. E., Staelin, D. H., & Hutter, D. J. 1988, A&A, 193, 357
Tsuji, T. 1978, PASJ, 30, 435
Tuthill, P. G. 1994, Ph.D. thesis, Univ. of Cambridge
van Belle, G. T., Dyck, H. M., Benson, J. A., & Lacasse, M. G. 1996, AJ, 112, 2147
Walker, M. F. 1958, ApJ, 128, 562